Passive Virtual Fixtures Adaptation in Minimally Invasive Robotic Surgery

Mario Selvaggio, *Student Member, IEEE*, Giuseppe Andrea Fontanelli, *Student Member, IEEE*, Fanny Ficuciello, *Senior Member, IEEE*, Luigi Villani, *Senior Member, IEEE* and Bruno Siciliano, *Fellow, IEEE*

***Abstract*—During robot-aided surgical interventions, the surgeon can benefit from the application of virtual fixtures (VFs). Though very effective, this technique is very often not practicable in unstructured surgical environments. In order to comply with the environmental deformation, both the VF geometry and the constraint enforcement parameters need to be online defined/adapted. This paper proposes a strategy for an effective use of VF assistance in minimally invasive robotic surgical tasks. An online VF generation technique based on the interaction force measurements is presented. Pose and geometry adaptations of the VF are considered. Passivity of the overall system is guaranteed by using energy tanks passivity-based control. The proposed method is validated through experiments on the da Vinci Research Kit.**

***Index Terms*—Surgical Robotics: Laparoscopy; Compliance and Impedance Control; Physical Human-Robot Interaction.**

I. Introduction

ROBOT-aided surgery permits filtering the surgeon's hand tremors and scaling down motions in order to make highly precise and dexterous movements inside the patient's body. This allows reducing trauma and postoperative pains which, in turn, results in significantly faster recovery time for patients.

In recent years, the application of shared-control techniques to robotic surgical interventions started to be investigated. Among these techniques, the use of virtual fixtures (VFs) has been identified as one of the most promising approaches [1]. VFs are software generated constraints which restrict the motion of a robotic manipulator into predefined regions or constrain it to move along a preplanned path [2]. This allows improving the operator's performance by reducing the mental workload, increasing the precision and/or decreasing the task completion time.

A wide variety of surgical tasks can benefit from the use of VFs, such as percutaneous needle insertion, femur cutting for prosthetic implant, suturing. However, the main drawback of this methodology is the strong task dependency: switching among even structured tasks would require interruptions and reprogramming of the system. Moreover, unstructured environments pose additional challenges to the VFs application. For instance, in minimally invasive robotic surgery the environment is deformable due to the flexibility of the organs and this makes the precomputed VF techniques hardly practicable.

A. Problem statement

Automatic VF generation/adaptation can be performed by exploiting vision-based techniques [3], [4]. Vision systems allow tracking organs as they move or deform. However, this can be a demanding task, particularly in cases where surgical targets have few structural features for tracking. Alternatively, force controlled exploration of patient-specific anatomy can be a time consuming procedure and thus not practicable in some surgical interventions [5]. Whatever method is used to generate them, to be effective in the surgical scenario, VFs must be adapted online as the environment moves or deforms, *i.e.* they must be repositioned and/or opportunely refined in order to reflect the different environmental configuration. Very few papers make a significant consideration of *adaptive* VF, where the constraint geometry (semi-)autonomously moves as a result of environmental changes.

On the other hand, guaranteeing a stable behavior of the robot endowed with adaptive VF control is of a paramount importance in robotic surgery. Interactive VF application results in variable impedance controllers that could threaten the stability of the robotic system [6], [7]. The analysis of the system behavior is complicated by the interaction with the user which further contributes to the overall system impedance parameters variation. Thus, passivity-based control techniques need to be exploited in order to ensure the safe use of the system for every change in the impedance parameters. In other words, during VF adaptation the robot must asymptotically converge towards an equilibrium point.

B. Related Works

Related works in this field can be separated into two main topics: *1) adaptive virtual fixtures*, *2) passivity-based control*.

1) Adaptive virtual fixtures: historically, robotic teleoperation systems have made use of VF as a perceptual overlay to enhance the human experience in performing remote manipulation tasks. Rosenberg pioneered VF in his work [8]. Since then, renewed interest has been shown in their use for robotic surgical procedures. In [9] the first attempt to transfer VF to the operating room is shown. The authors used VF

Manuscript received: February, 24, 2018; Revised May, 21, 2018; Accepted June, 5, 2018.

This paper was recommended for publication by Editor Ken Masamune upon evaluation of the Associate Editor and Reviewers' comments. This work was supported by the EC Seventh Framework Programme (FP7) within RoDyMan project 320992 and by the STAR 2016 Programme within MUSHA project.

The authors are with the Department of Information Technology and Electrical Engineering and with the Interdepartmental Center for Advances in Robotic Surgery, University of Naples Federico II, via Claudio, 21, 80125 Naples, Italy. E-mail: {mario.selvaggio}@unina.it

Digital Object Identifier (DOI): see top of this page.

generated from preoperative computed tomography images and constrained the motions of a surgical robot to a predefined path during the dissection of the internal mammary artery. Interactive generation of VF in surgical applications has been addressed in [10] where constrained optimization is used to enforce the VF constraint with objective function derived by user inputs.

More recently, it has been shown that VF can be opportunely generated using scans of the area of interest [11], [12]. A dynamic VF technique to enhance the surgical operation accuracy of admittance-type medical robots in deforming environments is presented in [13]: the target deformation is tracked actively and the proxy motion is constrained on a deforming sphere to simulate the beating heart surgery environment. One of the major obstacles in implementing vision generated VF in surgical applications is the organs displacement and deformation: whether the constraint geometry is defined preoperatively or intraoperatively, it must be mapped correctly to the organs as they move or deform.

Alternatively, VF may be opportunely adapted according to the currently being executed task or on the estimation of surgeon's skills. Learning from demonstration has been used for task dependent VFs application in [14], whereas adaptive VFs, based on the surgeon's level of expertise, are shown in [15]. An algorithm to select an appropriate admittance ratio based on the nature of the task was developed in [16]: automatic admittance ratio tuning is recommended for an efficient use of VFs. A method for online task tracking and on the use of adaptive VFs that can cope with their inherent inflexibility is presented in [17].

2) Passivity-based control: few authors have addressed the stability issues caused by VF adaptation as this can threaten the system stability. In [18] the authors applied and experimentally validated a non-energy-storing class of dynamic guidance VFs that do not suffer from internal energy accumulation. Utilizing a friction model to enforce constraints ensures that energy is not accumulated into the system [19]. However, frictional constraints suffer from problems related to forbidden regions replication. Redirection of VF forces in surgical robotics based on a passivity preserving condition has been presented in [20]. Stability of the closed-loop system can be investigated using the small-gain theorem: a sufficient condition, that guarantees stability in the presence of time-varying communication delay, is derived in [15]. Variable impedance/admittance control of robotic manipulators makes largely use of passivity-based control techniques to stabilize the system. An interesting approach relies on the concept of energy tanks and has been effectively used in [6], [7], [21]. The energy tanks approach is particularly suitable for the teleoperation, where large damping factors may degrade the transparency of the bilateral telerobotic system.

C. Contribution

This paper presents a methodology for online interactive generation and passive adaptation of VF for robotic assisted surgical interventions. More specifically, we propose:

- a VF pose and geometry adaptation strategy that uses a human-in-the-loop VF generation technique;
- an energy tanks passivity-based control method that ensures a stable system behavior.

The proposed methodology is validated through experiments performed on the da Vinci Research Kit (dVRK) [22], in which surgical dissection tasks have been considered.

The remainder of the paper is organized as follows: in Sect. II we present preliminary methods used in our implementation; Section III contains VF generation and adaptation techniques; Section IV shows the energy tanks passivity-based control; Section V contains the performed experiments and results alongside a discussion; Section VI concludes the paper.

II. Preliminaries

In this section we illustrate the methods used for the implementation of VFs to generic teleoperated robotic systems.

A. Robot Impedance Control

A very common practice in robotic teleoperation is to have an admittance/impedance controlled master robot. Considering a n degree-of-freedom (DoF) manipulator and defining a task space vector $\boldsymbol{x} \in \mathbb{R}^r$, with $r \leq n$, the following impedance dynamics can be achieved through control

$$\boldsymbol{M}\ddot{\tilde{\boldsymbol{x}}} + \boldsymbol{D}\dot{\tilde{\boldsymbol{x}}} = \boldsymbol{f}_{\mathrm{h}} + \boldsymbol{f}_{\mathrm{vf}}(\cdot), \tag{1}$$

where $\tilde{\boldsymbol{x}} = \boldsymbol{x}_{\mathrm{d}} - \boldsymbol{x}$, with $\boldsymbol{x}_{\mathrm{d}}$ being the desired value for the robot task space variable, $\boldsymbol{M} \in \mathbb{R}^{r\times r}$ and $\boldsymbol{D} \in \mathbb{R}^{r\times r}$ are inertia and damping matrices respectively, usually designed to be fixed, diagonal and positive definite, $\boldsymbol{f}_{\mathrm{h}} \in \mathbb{R}^r$ is the vector of the external forces applied by an interacting user and $\boldsymbol{f}_{\mathrm{vf}}(\cdot)$ is the additional force due to the possible presence of VFs. The above dynamics can be obtained by setting the torque control input $\boldsymbol{\tau} \in \mathbb{R}^n$ of the master robot as (see [23] for more details)

$$\boldsymbol{\tau} = \boldsymbol{B}(\boldsymbol{q})\boldsymbol{v} + \boldsymbol{N}(\boldsymbol{q},\dot{\boldsymbol{q}}) + \boldsymbol{J}^{\mathrm{T}}(\boldsymbol{q})\boldsymbol{f}_{\mathrm{h}} \tag{2}$$

$$\boldsymbol{v} = \boldsymbol{J}_{\mathrm{A}}^{-1}(\boldsymbol{q})\boldsymbol{M}^{-1}(\boldsymbol{M}\ddot{\boldsymbol{x}}_d + \boldsymbol{D}\dot{\tilde{\boldsymbol{x}}} - \boldsymbol{M}\dot{\boldsymbol{J}}_{\mathrm{A}}(\boldsymbol{q},\dot{\boldsymbol{q}})\dot{\boldsymbol{q}} - \boldsymbol{f}_{\mathrm{h,A}}), \tag{3}$$

where $\boldsymbol{B}(\boldsymbol{q}) \in \mathbb{R}^{n\times n}$ is the joint space inertia matrix, $\boldsymbol{J}(\boldsymbol{q})$, $\boldsymbol{J}_{\mathrm{A}}(\boldsymbol{q}) \in \mathbb{R}^{r\times n}$ are the geometric and the analytical Jacobians, respectively, and

$$\boldsymbol{N}(\boldsymbol{q},\dot{\boldsymbol{q}}) = \boldsymbol{C}(\boldsymbol{q},\dot{\boldsymbol{q}})\dot{\boldsymbol{q}} + \boldsymbol{g}(\boldsymbol{q}) + \boldsymbol{h}(\boldsymbol{q},\dot{\boldsymbol{q}}) \tag{4}$$

accounts for Coriolis and centrifugal contributions $\left(\boldsymbol{C}(\boldsymbol{q},\dot{\boldsymbol{q}})\dot{\boldsymbol{q}}\right)$, gravity $\left(\boldsymbol{g}(\boldsymbol{q})\right)$, friction and other disturbance torques $\left(\boldsymbol{h}(\boldsymbol{q},\dot{\boldsymbol{q}})\right)$. Notice that the term $\boldsymbol{f}_{\mathrm{h,A}}$ differs from $\boldsymbol{f}_{\mathrm{h}}$ by a mapping, depending on the orientation representation.

B. External force estimation

Equation (2) requires the measurement of the external forces $\boldsymbol{f}_{\mathrm{h}}$. When they are not directly measurable, force estimation could be performed by resorting to a nonlinear dynamic observer [24], [25]. This method allows the estimation of unknown external forces without the need of measuring the usually noisy acceleration signal.

In greater details, considering the measured torque vector $\boldsymbol{\tau}_r \in \mathbb{R}^n$, a residual vector can be defined as follows

$$\boldsymbol{r}(t) = \boldsymbol{K}_I\left(\boldsymbol{B}(\boldsymbol{q})\dot{\boldsymbol{q}} - \int_0^t \left(\boldsymbol{r}(\sigma) + \boldsymbol{\tau}_r + \tilde{\boldsymbol{N}}(\boldsymbol{q},\dot{\boldsymbol{q}})\,d\sigma\right)\right), \tag{5}$$

where $\boldsymbol{K}_I$ is a diagonal and positive definite gain matrix and

$$\tilde{\boldsymbol{N}}(\boldsymbol{q},\dot{\boldsymbol{q}}) = \boldsymbol{C}^T(\boldsymbol{q},\dot{\boldsymbol{q}})\dot{\boldsymbol{q}} - \boldsymbol{g}(\boldsymbol{q}) - \boldsymbol{h}(\boldsymbol{q},\dot{\boldsymbol{q}}). \tag{6}$$

Hence, the estimated external forces $\hat{\boldsymbol{f}}_{\mathrm{h}}$ can computed using the following equality

$$\hat{\boldsymbol{f}}_{\mathrm{h}} = \boldsymbol{J}^{-T}(\boldsymbol{q})\,\boldsymbol{r}, \tag{7}$$

where $\boldsymbol{J}^{-T}(\boldsymbol{q})$ denotes the generalized inverse of the robot Jacobian transpose. Hereafter, we will consider $\boldsymbol{f}_{\mathrm{h}} = \hat{\boldsymbol{f}}_{\mathrm{h}}$.

C. Virtual Fixtures

VFs can be classified into two main classes: forbidden-region virtual fixtures (FRVF) and guidance virtual fixtures (GVF) [2]. Generally speaking, FRVF are suitable for simulating barriers, constraining surfaces or delicate regions that the user should be forbidden to enter. In contrast, a GVF has an attractive behavior that pulls the robot end-effector towards a desired path (see Fig. 1).

In this work, we focus on the latter VF type (hereafter, we will refer to GVF simply as VF). Two quantities are essential to describe a VF: its *geometry* and the *constraint enforcement* method.

1) VF geometry model: a simple, yet general, way of geometrically formulating a smooth continuous VF is through parametric curves. Without loss of generality, we adopt cubic splines. In its 1-dimensional form, a cubic spline is defined by

$$\Gamma_i(s) = C_0 + C_1(s-x_i) + C_2(s-x_i)^2 + C_3(s-x_i)^3 \tag{8}$$

where $\Gamma_i(s)$ denotes the curve in its i-th interval $[x_i, x_{i+1}]$, $s \in [0,1]$ is the curve parameter, C_0, C_1, C_2, C_3 are constants determined by imposing four conditions (usually being boundary constraints $\Gamma_i(0), \Gamma_i(1), \Gamma_i'(0), \Gamma_i'(1)$, where $\Gamma_i'(\cdot)$ denotes the curve derivative w.r.t. the parameter s). As explained later in this work (Sect. III), we build the spline geometry by fitting a set of recorded interaction points. For this purpose, we use parabolically terminated splines.

2) VF constraint enforcement: a GVF exhibits attractive behavior towards the desired path. The simplest constraint enforcement method consists in applying a spring-damper like force. In the linear case this can be defined as follows

$$\boldsymbol{f}_{\mathrm{vf}}\left(\tilde{\boldsymbol{x}},\dot{\tilde{\boldsymbol{x}}}\right) = -\boldsymbol{K}_{\mathrm{vf}}\tilde{\boldsymbol{x}} - \boldsymbol{D}_{\mathrm{vf}}\dot{\tilde{\boldsymbol{x}}}, \tag{9}$$

where $\boldsymbol{K}_{\mathrm{vf}} \in \mathbb{R}^{r\times r}$ and $\boldsymbol{D}_{\mathrm{vf}} \in \mathbb{R}^{r\times r}$ are properly designed diagonal and positive definite matrices and $\boldsymbol{x}_{\mathrm{d}}$ is the set-point belonging to the constraint geometry having minimum distance from $\boldsymbol{x}$ (see Fig. 1). An impedance controlled manipulator (1), endowed with VF control forces defined in (9), exhibits a closed-loop behavior that can be described by

$$\boldsymbol{M}\ddot{\tilde{\boldsymbol{x}}} + \hat{\boldsymbol{D}}\dot{\tilde{\boldsymbol{x}}} + \boldsymbol{K}_{\mathrm{vf}}\tilde{\boldsymbol{x}} = \boldsymbol{f}_{\mathrm{h}}, \tag{10}$$

where $\hat{\boldsymbol{D}} = \boldsymbol{D} + \boldsymbol{D}_{\mathrm{vf}}$ contains the damping assigned both by the impedance control and the VF constraint enforcement method. The desired dynamics (10) can be easily obtained by adding the elastic and damping contributions shown in the right-hand side of (9) to the control input defined in (3).

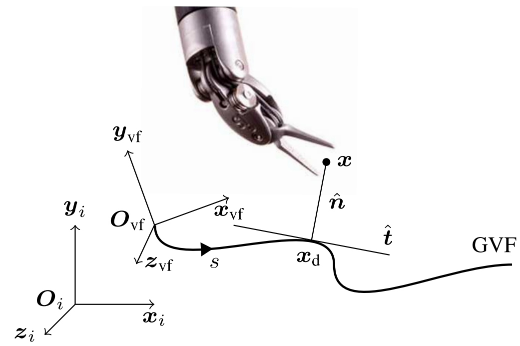

Fig. 1. Example of Guidance Virtual Fixture (GVF) spline geometry and minimum distance from the robot tool central point $\boldsymbol{x}$. $\hat{\boldsymbol{t}}$ and $\hat{\boldsymbol{n}}$ denote the tangent and the normal directions, respectively, with origin in $\boldsymbol{x}_{\mathrm{d}}$, *i.e.*, the $\boldsymbol{x}$ nearest point on the curve. $\mathcal{F}_i : \{\boldsymbol{O}_i; \boldsymbol{x}_{\mathbf{i}}, \boldsymbol{y}_{\mathbf{i}}, \boldsymbol{z}_{\mathbf{i}}\}$ = inertial frame, $\mathcal{F}_{\mathrm{vf}} : \{\boldsymbol{O}_{\mathrm{vf}}; \boldsymbol{x}_{\mathrm{vf}}, \boldsymbol{y}_{\mathrm{vf}}, \boldsymbol{z}_{\mathrm{vf}}\}$ = virtual fixture frame.

D. Minimun distance

For cubic splines, described by (8), there does not exist an analytical solution to the problem of minimum Euclidean distance computation. However, this problem can be tackled by resorting to iterative methods, such as Newton-Raphson (NR). This represents a general method of finding the extrema (minima or maxima) of a given function in an iterative manner. Our goal is to find the spline parameter $\bar{s}$ corresponding to the minimum distance point $\boldsymbol{x}_{\mathrm{d}} = \Gamma(\bar{s})$. For this purpose, starting from a generic initial condition $s_0 \in [0,1]$, we use the customary NR update law

$$s_{k+1} = s_k + \frac{\delta(\boldsymbol{x}, s_k)}{\delta'(\boldsymbol{x}, s_k)}, \tag{11}$$

where $\delta(\boldsymbol{x}, s) : \mathbb{R}^r \times \mathbb{R} \to \mathbb{R}$ is the distance function between a point $\boldsymbol{x}$ and the spline $\Gamma(s)$, that is given by

$$\delta(\boldsymbol{x}, s) = \sqrt{\left(\boldsymbol{x} - \Gamma(s)\right)^{\mathrm{T}}\left(\boldsymbol{x} - \Gamma(s)\right)} \tag{12}$$

and $\delta'(\boldsymbol{x}, s_k)$ denotes the derivative at s_k of (12) with respect to the curve parameter s.[1]

III. Virtual Fixture Generation and Adaptation

We now proceed to describe the VF *generation* technique and the *adaptation* strategies.

A. VF generation

Our aim is to let the user interactively program VFs for interaction tasks (*e.g.* surgical dissections). Among many other choices, we adopt the policy of recording a set of interaction points that are then used to build the VF geometry. In this way, the surgeon is given the ability to program the VF geometric path by simply interacting with the environment. Interaction detection is possible by measuring forces at the slave side. Recorded points are then fitted through a penalized regression spline fitting algorithm in which coefficients of (8) are obtained by minimizing the sum of least squares plus a

[1] Although computationally very efficient, NR method can converge to local maxima/minima. To tackle this problem, we use the previously determined $\bar{s}$ as initial guess for the next minimum distance query. We empirically found this method to be effective for our scope.

penalty function which suppresses nonlinearity and controls the curve smoothing. Mathematically, the problem is described by

$$\Gamma(s) = \arg\min_{\Gamma(s)} \left(\sum_i (y_i - \Gamma(s_i))^2 + \lambda \int (\Gamma''(s))^2 ds \right) \qquad (13)$$

where λ is the regularization parameter that penalizes nonlinearities in the path, y_i is the i-th recorded interaction point and $\Gamma''(s)$ is the curve second derivative of $\Gamma(s)$ with respect to its parameter s.

B. VF adaptation

To adapt a VF preserving the proposed human-in-the-loop approach, a non linear and time varying stiffness profile is adopted for $\boldsymbol{K}_{\text{vf}}$ in (10). This is used to both limit the spatial and the temporal influence of a VF. More specifically, we design each non-zero entry of the stiffness matrix to be

$$k_{\text{vf,ii}}(\tilde{x}, t) = \beta(\tilde{x}, t) K_{\text{max}} \quad \forall\, i = 1, \dots, r \qquad (14)$$

where $k_{\text{vf,ii}}$ is the (i,i) entry of the $\boldsymbol{K}_{\text{vf}}$ matrix, $\beta(\tilde{x}, t)$ is an impedance shaping function, t denotes time and K_{max} is the maximum stiffness value adopted. The definition of $\beta(\tilde{x}, t)$ allows to realize different adaptation strategies as detailed in the following two sections.

1) Pose adaptation: the pose adaptation strategy consists in positioning a predefined VF geometry into a desired location. With reference to Fig. 1 the problem is to define a desired reference frame $\mathcal{F}_{\text{vf,d}} : \{\boldsymbol{O}_{\text{vf,d}}; \boldsymbol{x}_{\text{vf,d}}, \boldsymbol{y}_{\text{vf,d}}, \boldsymbol{z}_{\text{vf,d}}\}$ to which the current VF reference frame $\mathcal{F}_{\text{vf}} : \{\boldsymbol{O}_{\text{vf}}; \boldsymbol{x}_{\text{vf}}, \boldsymbol{y}_{\text{vf}}, \boldsymbol{z}_{\text{vf}}\}$ must converge to. As explained, to make this procedure interactive for the user, we adopt the policy of recording a set of slave robot interaction points with the environment that are then used to fit the predefined geometry. To allow the user to freely record new interaction points, we found convenient to limit the spatial influence of the current VF adopting the $\beta(\tilde{x})$ function qualitatively depicted in Fig. 2: this function allows the operator to easily exit the VF constraining zone and freely record new interaction points as sought. For each task space variable $\beta(\tilde{x})$ is mathematically described by

$$\beta(\tilde{x}) = \begin{cases} 0 & \text{if } |\tilde{x}| \geq l \\ \dfrac{1}{2}\left(1 + \cos\left(\dfrac{\pi(|\tilde{x}| - d)}{l - d}\right)\right) & \text{otherwise} \\ 1 & \text{if } |\tilde{x}| \leq d \end{cases} \qquad (15)$$

where l is the distance at which the VF attractive action vanishes completely and d is the threshold distance value inside which the stiffness perceived is K_{max}. Once a set of recorded interaction points is available, the classical least-squares minimization method is used to fit the predefined geometry onto it. This gives the desired VF pose that minimizes the sum of squared residuals between the VF from the point set, *i.e.* $\mathcal{F}_{\text{vf,d}}$. This pose is then tracked online by suitably defining the pose error between $\mathcal{F}_{\text{vf,d}}$ and $\mathcal{F}_{\text{vf}}$ frames. Indicating with $\boldsymbol{R} = [\boldsymbol{n}, \boldsymbol{s}, \boldsymbol{a}]$ and $\boldsymbol{R}_d = [\boldsymbol{n}_d, \boldsymbol{s}_d, \boldsymbol{a}_d]$ the rotation matrices associated with $\mathcal{F}_{\text{vf}}$ and $\mathcal{F}_{\text{vf,d}}$, respectively, the error can be written as follows (see [23])

$$\boldsymbol{e} = \begin{bmatrix} \boldsymbol{e}_P \\ \boldsymbol{e}_O \end{bmatrix} = \begin{bmatrix} \boldsymbol{O}_{\text{vf,d}} - \boldsymbol{O}_{\text{vf}} \\ \frac{1}{2}(\boldsymbol{n} \times \boldsymbol{n}_d + \boldsymbol{s} \times \boldsymbol{s}_d + \boldsymbol{a} \times \boldsymbol{a}_d) \end{bmatrix}, \qquad (16)$$

where $\boldsymbol{O}_{\text{vf,d}}$ and $\boldsymbol{O}_{\text{vf}} \in \mathbb{R}^3$ denote the desired and current frame origins, respectively. A simple proportional control law defined on the error in (16) allows it to asymptotically converge to zero guaranteeing a smooth regulation behavior. The resulting error dynamics can be written as follows

$$\dot{\boldsymbol{e}} + \boldsymbol{\Lambda}_p \boldsymbol{e} = 0 \qquad \boldsymbol{\Lambda}_p > 0, \qquad (17)$$

where $\boldsymbol{\Lambda}_p$ is a positive definite diagonal matrix containing control gains that are numerically different to account the non-homogeneous dimensions of the error blocks.

2) Geometry adaptation: The geometry adaptation strategy consists in transforming the current VF geometry into a desired one.

We suppose that the user is performing a task aided by the currently active VF and necessarily needs to deviate, *e.g.* to comply with the environment deformation. The same interaction points fitting strategy used for the VF generation (see Sect. III-A) can be used to define a new desired geometry. In this case, the user may want to completely deactivate the current VF to freely record new interaction points. To let the impedance parameters of the former VF to gradually vanish, we use the following temporal variation of the stiffness

$$\beta(t) = \frac{1}{2}\left(1 + \cos\left(\frac{\pi(t - t_s)}{t_i - t_s}\right)\right) \quad t_s < t < t_i \qquad (18)$$

where t_s, t_i are the starting and final instant of the stiffness variation time interval. Once a new desired geometry has been defined, the problem is to redirect the robot tool central point $\boldsymbol{x}$ towards the new VF.

To achieve a smooth behavior of the system, we let the impedance parameters gradually materialize. This is realized by the following temporal stiffness variation

$$\beta(t) = \frac{1}{2}\left(1 - \cos\left(\frac{\pi(t - t_i)}{t_f - t_i}\right)\right) \quad t_i < t < t_f \qquad (19)$$

where t_i, t_f are initial and final instants of the positive impedance variation, respectively. To activate/deactivate the VF according to the stiffness variation laws (18) and (19) different strategies can be adopted. We decided to associate this functionality to the pressing of a dVRK console foot pedal.

It is worth noting that the proposed impedance variation strategy can be also employed to smoothly apply a VF or switch between two of them: switching the attraction point $\boldsymbol{x}_d$ from one VF to another, when the stiffness reaches zero, guarantees a smooth transition of the system. From a passivity point of view this translates in not generating additional energy into the system.

IV. Energy Tanks Passivity-Based Control

We now proceed analyzing the system passivity when subject to the proposed impedance variations (see Sect. III-B). The following definition of passivity is used

Definition 1. *A system with state space model $\dot{\boldsymbol{x}} = f(\boldsymbol{x}, \boldsymbol{u}) \in \mathbb{R}^q$, with initial state $\boldsymbol{x}(0) = \boldsymbol{x}_0 \in \mathbb{R}^q$, input vector $\boldsymbol{u} \in \mathbb{R}^l$ and output $\boldsymbol{y} = h(\boldsymbol{x}, \boldsymbol{u})$ is said to be passive if there exists*

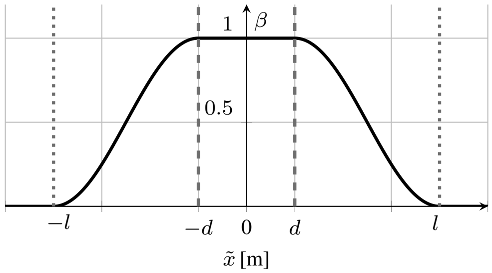

Fig. 2. VF impedance shaping function $\beta(\tilde{x})$ used to limit the VF spatial influence. $\tilde{x}$ denotes the difference between the desired and current value or the master task space variable.

a positive semidefinite function $\mathcal{S} : \mathbb{R}^q \to \mathbb{R}_+$, called storage function, such that

$$\mathcal{S}\left(\boldsymbol{x}\left(T\right)\right) - \mathcal{S}\left(\boldsymbol{x}_0\right) \leq \int_0^t \boldsymbol{y}^{\mathrm{T}}\left(t\right)\boldsymbol{u}\left(t\right)dt \tag{20}$$

for all input signals $\boldsymbol{u} : [0, T] \to \mathbb{R}^l$, initial states $\boldsymbol{x}_0 \in \mathbb{R}^q$ and $T > 0$. Thus, proving passivity is equivalent to finding an appropriate storage function $\mathcal{S}\left(\boldsymbol{x}\right)$ such that

$$\dot{\mathcal{S}} \leq \boldsymbol{y}^{\mathrm{T}}\boldsymbol{u} \qquad \forall(\boldsymbol{x}, \boldsymbol{u}). \tag{21}$$

It can be easily noted that the model in (10) is not guaranteed to be passive w.r.t. the input-output pair ($\boldsymbol{f}_{\mathrm{h}}$,$\dot{\tilde{\boldsymbol{x}}}$) if we consider as storage function the system energy

$$H(\tilde{\boldsymbol{x}}, \dot{\tilde{\boldsymbol{x}}}) = \frac{1}{2}\dot{\tilde{\boldsymbol{x}}}^{\mathrm{T}}\boldsymbol{M}\dot{\tilde{\boldsymbol{x}}} + \frac{1}{2}\tilde{\boldsymbol{x}}^{\mathrm{T}}\boldsymbol{K}_{\mathrm{vf}}\tilde{\boldsymbol{x}}, \tag{22}$$

where $\boldsymbol{M}$, and $\boldsymbol{K}_{\mathrm{vf}}$ have been defined in Sect. II. Indeed, the time derivative of (22) (assuming that $\boldsymbol{M}$ remains constant over time) can be written as follows (omitting arguments of $H(\tilde{\boldsymbol{x}}, \dot{\tilde{\boldsymbol{x}}})$)

$$\dot{H} = \dot{\tilde{\boldsymbol{x}}}^{\mathrm{T}}\boldsymbol{M}\ddot{\tilde{\boldsymbol{x}}} + \tilde{\boldsymbol{x}}^{\mathrm{T}}\boldsymbol{K}_{\mathrm{vf}}\dot{\tilde{\boldsymbol{x}}} + \frac{1}{2}\tilde{\boldsymbol{x}}^{\mathrm{T}}\dot{\boldsymbol{K}}_{\mathrm{vf}}\tilde{\boldsymbol{x}}, \tag{23}$$

which, evaluated along the system trajectories, becomes

$$\dot{H} = \dot{\tilde{\boldsymbol{x}}}^{\mathrm{T}}\boldsymbol{f}_{\mathrm{h}} - \dot{\tilde{\boldsymbol{x}}}^{\mathrm{T}}\hat{\boldsymbol{D}}\dot{\tilde{\boldsymbol{x}}} + \frac{1}{2}\tilde{\boldsymbol{x}}^{\mathrm{T}}\dot{\boldsymbol{K}}_{\mathrm{vf}}\tilde{\boldsymbol{x}}. \tag{24}$$

Since $\dot{\boldsymbol{K}}_{\mathrm{vf}}$ can have both positive and negative eigenvalues, a sufficient, yet conservative, condition to satisfy (21) is to have a negative semidefinite $\dot{\boldsymbol{K}}_{\mathrm{vf}}$ in (24).

A possible solution to this problem is to design a passivity preserving controller that tracks the desired stiffness profile while limiting its change when condition (21) is violated. To this end, we exploit the concept of energy tanks, introduced in [26], which aim at recovering the dissipated energy of the system to implement a less conservative impedance variation without violating the overall passivity of the system. To this end, the master side manipulator is endowed with an energy storing element having the following storage function

$$T\left(z\right) = \frac{1}{2}z^2, \tag{25}$$

whose dynamics is described by the following equation

$$\dot{z} = \frac{\varphi}{z}\dot{\tilde{\boldsymbol{x}}}^{\mathrm{T}}\hat{\boldsymbol{D}}\dot{\tilde{\boldsymbol{x}}} - \frac{\gamma}{z}\frac{1}{2}\tilde{\boldsymbol{x}}^{\mathrm{T}}\dot{\boldsymbol{K}}_{\mathrm{vf}}\tilde{\boldsymbol{x}}, \tag{26}$$

with $z \in \mathbb{R}$ being the state of the tank and $\varphi, \gamma \in \{0, 1\}$ are parameters used to enforce the upper bound limitation $\bar{T}$ for

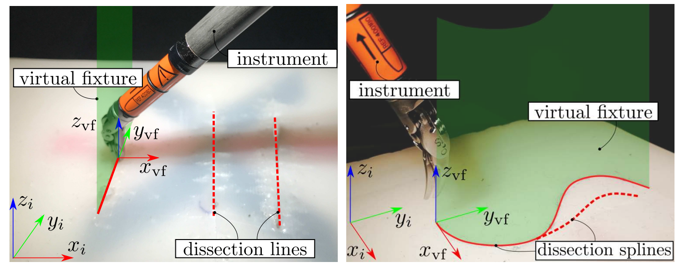

(a) Linear dissection tasks with VF pose adaptation.
(b) Curvilinear dissection task with VF geometry adaptation.

Fig. 3. Experimental setup and tasks.

the energy stored in the tank [27]. We note that (26) is singular for $z = 0$, thus a lower threshold ε for the tank energy must also be set.

Thus, the extended dynamics can be rewritten as follows

$$\begin{cases} \boldsymbol{M}\ddot{\tilde{\boldsymbol{x}}} + \hat{\boldsymbol{D}}\dot{\tilde{\boldsymbol{x}}} + \boldsymbol{K}_{\mathrm{vf}}\tilde{\boldsymbol{x}} = \boldsymbol{f}_{\mathrm{h}} \\ \dot{\boldsymbol{K}}_{\mathrm{vf}} = \alpha\left(\boldsymbol{\Lambda}_k\left(\boldsymbol{K}_{\mathrm{vf,d}} - \boldsymbol{K}_{\mathrm{vf}}\right) + \dot{\boldsymbol{K}}_{\mathrm{vf,d}}\right) \\ \dot{z} = \frac{\varphi}{z}\dot{\tilde{\boldsymbol{x}}}^{\mathrm{T}}\hat{\boldsymbol{D}}\dot{\tilde{\boldsymbol{x}}} - \frac{\gamma}{z}\frac{1}{2}\tilde{\boldsymbol{x}}^{\mathrm{T}}\dot{\boldsymbol{K}}_{\mathrm{vf}}\tilde{\boldsymbol{x}} \end{cases}, \tag{27}$$

where $\boldsymbol{\Lambda}_k \in \mathbb{R}^{r\times r}$ is a diagonal and positive definite matrix containing the stiffness tracking control parameter and $\alpha \in \{0, 1\}$ is a variable used to activate/deactivate the stiffness variation in case of passivity violation. The master system, endowed with the energy tank, has the following energy function

$$\mathcal{H} = H + T = \frac{1}{2}\dot{\tilde{\boldsymbol{x}}}^{\mathrm{T}}\boldsymbol{M}\dot{\tilde{\boldsymbol{x}}} + \frac{1}{2}\tilde{\boldsymbol{x}}^{\mathrm{T}}\boldsymbol{K}_{\mathrm{vf}}\tilde{\boldsymbol{x}} + \frac{1}{2}z^2, \tag{28}$$

whose time derivative is given by

$$\dot{\mathcal{H}} = \dot{H} + \dot{T} = \dot{\tilde{\boldsymbol{x}}}^{\mathrm{T}}\boldsymbol{M}\ddot{\tilde{\boldsymbol{x}}} + \tilde{\boldsymbol{x}}^{\mathrm{T}}\boldsymbol{K}_{\mathrm{vf}}\dot{\tilde{\boldsymbol{x}}} + \frac{1}{2}\tilde{\boldsymbol{x}}^{\mathrm{T}}\dot{\boldsymbol{K}}_{\mathrm{vf}}\tilde{\boldsymbol{x}} + z\dot{z} \tag{29}$$

which, evaluated along the system trajectories, becomes

$$\dot{\mathcal{H}} = \dot{\tilde{\boldsymbol{x}}}^{\mathrm{T}}\boldsymbol{f}_{\mathrm{h}} - (1-\varphi)\,\dot{\tilde{\boldsymbol{x}}}^{\mathrm{T}}\hat{\boldsymbol{D}}\dot{\tilde{\boldsymbol{x}}} + (1-\gamma)\,\frac{1}{2}\tilde{\boldsymbol{x}}^{\mathrm{T}}\dot{\boldsymbol{K}}_{\mathrm{vf}}\tilde{\boldsymbol{x}}. \tag{30}$$

By defining the following control laws for α, φ and γ

$$\alpha = \begin{cases} 0 & \text{if } T \leq \varepsilon \ \& \ \dot{\boldsymbol{K}}_{\mathrm{vf}} > 0 \\ 1 & \text{otherwise} \end{cases} \qquad \gamma = \begin{cases} \varphi & \text{if } \dot{\boldsymbol{K}}_{\mathrm{vf}} < 0 \\ 1 & \text{otherwise} \end{cases}$$
$$\varphi = \begin{cases} 1 & \text{if } T \leq \bar{T} \\ 0 & \text{otherwise} \end{cases} \tag{31}$$

the system in (27) is passive with respect to the input-output pair ($\boldsymbol{f}_{\mathrm{h}}$,$\dot{\tilde{\boldsymbol{x}}}$) with storage function (28). Indeed, it can be easily verified that (30) always satisfies the condition (21).

V. Experiments and Results

We now describe the experimental setup and present the VF pose and geometry adaptation experiments.

A. Experimental setup

The experiments have been performed on the dVRK platform. The robot has been used in teleoperation mode, with one Patient Side Manipulator (PSM) commanded by one Master Tool Manipulator (MTM). The MTM has been controlled using impedance control inputs described in Sect. II-A with

$m_{ii} = 1.5$, $d_{ii} = 0$ being the (i, i) entries of the matrices $\boldsymbol{M}$ and $\boldsymbol{D}$, respectively. The dVRK dynamic parameters used in (2) had been previously identified in [28]. The application of torque inputs has been possible thanks to the open-source hardware and software architecture developed by [29]. Given the discrete-time implementation and in order to have a critically damped system behavior, the $\boldsymbol{D}_{\text{vf}}$ has been adapted according to the stiffness variation such that $d_{\text{vf},ii} = 2\sqrt{m_{ii} k_{\text{vf},ii}}$ where $d_{\text{vf},ii}$ and $k_{\text{vf},ii}$ are the (i, i) entries of the matrices $\boldsymbol{D}_{\text{vf}}$ and $\boldsymbol{K}_{\text{vf}}$, respectively. Forces at the slave side have been measured making use of the dVRK trocar force sensor developed in [30]. The object used for experiments is a silicon rubber phantom commonly used by surgeons for training. It has been placed on a plastic 3D printed support. The fitting algorithm described by (13) has been implemented using the ALGLIB library [31]. The values of the β function limits in (15) have been fixed to $d = 0.005\,\text{m}$ and $l = 0.02\,\text{m}$, while $t_i = t_f = 2.5\,\text{s}$ in (18) and (19). The maximum stiffness has fixed to $K_{\text{vf,max}} = 600\,\text{N/m}$.

The energy tank upper threshold has been chosen as $\bar{T} = 0.01$ J while the lower threshold, has been set to $\varepsilon = 0.002$ J. The gap between these two quantities has been designed according to the maximum potential energy that is possible to store using the proposed $\beta(\tilde{x})$ function (see Fig. 2), *i.e.* $E_{\text{p,max}} = 1/2 K_{\text{vf,max}} d^2$. The VF control loop runs at $5\,\text{ms}$ while the teleoperation loop at $1\,\text{ms}$.

B. Pose adaptation experiment

The pose adaptation strategy (introduced in Sect. III-B1) is evaluated in multiple dissection tasks executed in spatially separated regions. Without loss of generality, we fix the geometry of the VF to be a spline representing a straight line. This particular choice is made to present clearer and more intuitive results of the pose adaptation. In this case, the fitting strategy for the VF geometry reduces to a linear regression problem where the desired $\boldsymbol{y}_{\text{vf,d}}$ axis of the $\mathcal{F}_{\text{vf,d}}$ reference frame is fitted using the last $n_p = 50$ recorded interaction poses of the slave robot with the environment. In addition, we leave the human operator free to move in the direction orthogonal to the phantom (see Fig. 3(a)). Every dissection task requires multiple interaction phases with the environment in which points are recorded. The VF pose is continuously updated by fitting these recorded points. With reference to Fig. 4 the experiment starts with the VF approximatively placed on the first dissection line. As soon as the robot starts interacting with the environment, the desired stiffness reaches the K_{max} value and the user is aided in accomplishing the first task by complying with the VF geometry. Around 20s the user switch to another task by exiting the current VF influence area ($|\tilde{x}| > l$). This can be seen in Fig. 4(e) in which we register a peak in the estimated force at the master side ($\approx 5\,\text{N}$) when the stiffness starts to decrease. Notice that this exiting is made possible by the $\beta(\tilde{x})$ function chosen in (15). During the subsequent time period, the user moves in free motion, *i.e.* $f_h \approx 0$ as it can be seen in Fig. 4(e) (time interval [20,25]s). A new interaction phase takes place in a spatially separated region at 25s. The new desired VF pose is calculated and the VF is updated following the method described in Sect. III-B1.

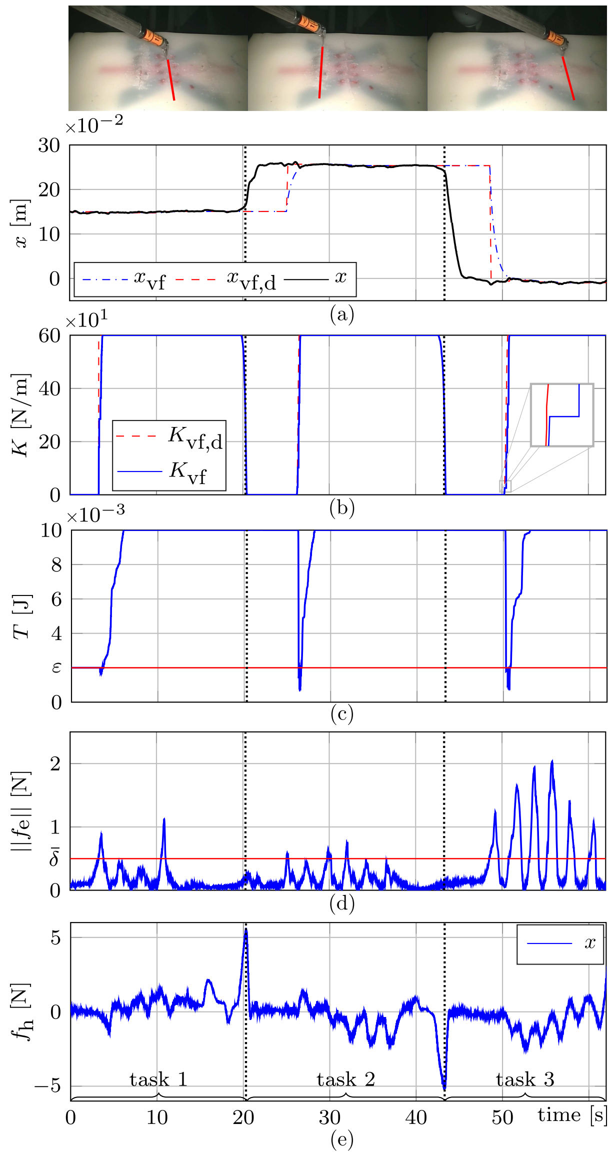

Fig. 4. VF pose adaptation experiment. Time histories of: (a) VF and tool central point pose along the x direction; (b) stiffness; (c) energy tank level; (d) slave interaction force; (e) human operator force on the master side.

Figure 4(d) shows the interaction force norm recorded at the slave side together with the chosen threshold $\bar{\delta} = 0.5$ N. This has been used to discriminate between interaction and free motion during the acquisition of points for the VF generation. Also note that, upon the starting of a new task, $x_{\text{vf,d}}$ changes significantly. However, the user does not experience guidance forces until the VF reaches the proximity of the master robot position. Indeed, only when $|\tilde{x}| < l$ the stiffness is increased. This effect is again produced by the chosen $\beta(\tilde{x})$ function (15). As mentioned in Sect. IV, the change in stiffness threatens the system passivity. The energy tank passivity-based control ensures a passive behavior by implementing the change in stiffness only when sufficient tank energy is at disposal. This is evident looking at Figs. 4(b) and 4(c). In particular, we can notice that the stiffness is kept constant (*i.e.* $\dot{K}_{\text{vf}} = 0$) when the tank is at its lower threshold until it gets replenished, thus not introducing discontinuities. This is made possible through the use of control laws given in (27) and (31). Fig. 4(b) contains

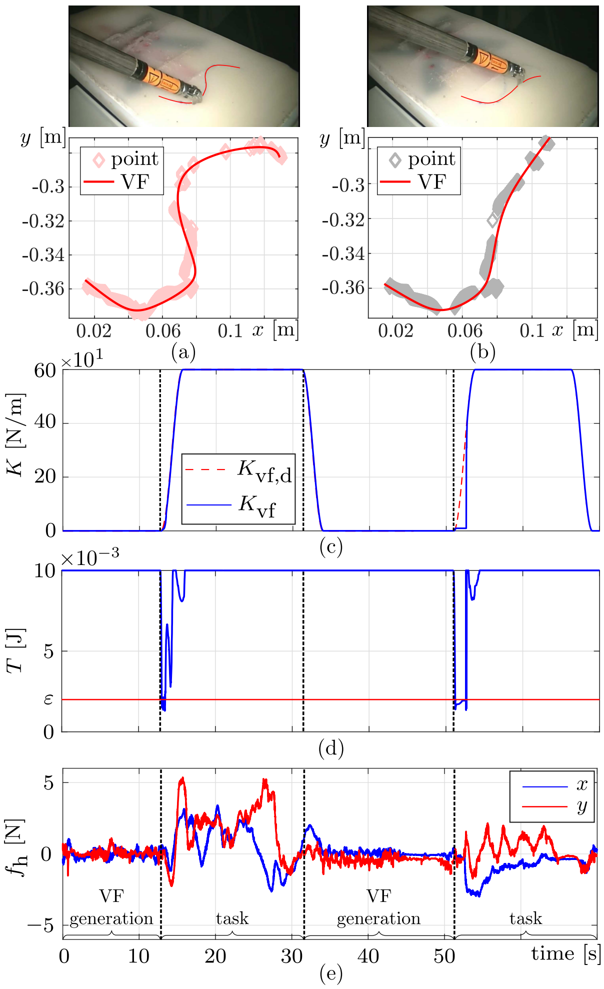

Fig. 5. Geometry adapation experiment. (a) First VF geometry generated by the recorded interaction points. (b) Second VF geometry. (c-e) Time histories of: (c) stiffness; (d) tank energy level; (e) human operator estimated force on the master side.

a focus around 50 s that emphasizes this behavior.

Finally, looking at the estimated forces in Fig. 4(e), it can be noticed that relatively high forces (≈ 5 N) are only applied at the task switching.

C. Geometry adaptation experiment

The geometry adaptation experiment consists in the refinement of a VF geometry to comply with a possible environmental change. We sought for a simple yet effective method to perform the VF geometry adaptation respecting the human-in-the-loop paradigm. This resulted in a procedure composed by the following steps: (i) the user can generate the desired VF geometry using the proposed interactive generation method presented in Sect. III-A; (ii) the user can activate the VF by pressing a foot pedal and start performing the task; (iii) the user may want to deviate from the previously defined path to comply with the environment/plan change; thus she/he can deactivate the current VF and freely record new interaction points for generating a new VF path; (iv) the user can activate the latest generated VF by releasing the foot pedal and be aided during the task completion. We have performed an experiment involving the above defined steps. Referring to Fig. 5, the experiment starts with the first VF generation (time interval $[0, 13]$ s) in which interaction points are recorded and the path is generated by the fitting algorithm[2]. The resulting VF geometry is shown in Fig. 5(a) as a solid red line, together with the corresponding interaction points (in pink). Subsequently, the VF is activated and the dissection task is started (time interval $[13, 32]$ s). During the task the surgeon decides to change the previously defined VF geometry to comply with a possible plan/environmental change. First, the current VF is deactivated and a new VF generation phase is undertaken (time interval $[32, 51]$ s). To deactivate the current VF the impedance is brought to zero following the variation law presented in (18) by pressing a foot pedal. Newly recorded points are fitted as explained in Sect. III-A to generate a new VF. The resulting VF geometry is represented in Fig. 5(b) as a solid red line together with interaction points in gray. The VF is then activated to complete the task (time interval $[51, 70]$ s). Figure. 5(c) contains the time history of the desired stiffness variation according to the laws (18) and (19). Even in this case, the passivity of the system is preserved by means of the energy tanks passivity-based control described in Sect. IV. Figure 5(d) contains the time evolution of the tank energy used to implement the stiffness variation. The effect of the passivity-based control action is evident in 5(c) (around time 51 s) where the tank is discharged and the stiffness is kept constant until it gets replenished. Finally, figure 5(e) shows human operator's estimated forces on the master side during the task execution: it can be seen that when the VF is activated the user is aided by guidance forces in performing the task.

A video showing both real and simulated experiments [32] is attached to this paper.

D. Discussion

When the impedance variation profile is known in advance, a state-independent stability constraint can be imposed [33]. However, this would imply the application of a fixed damping parameter on the system (opportunely defined on the basis of the maximum stiffness variation, *i.e.* worst case design) which degrades the system transparency when the bilateral teleoperation is enabled. The same applies to other passivity-based control techniques, such as the time domain passivity-based control approach [34]: here, the control action in the form of a dissipative element that absorbs the energy generated by the system causes, in general, the presence of higher damping on the system. These considerations motivated us to use the energy tanks passivity-based control approach.

We also note that the proposed VF path generation, that uses interaction points recording, constitutes a simple yet effective method of programming a VF path in real-time. This can be used whenever the desired path is not definable pre-operatively. For instance, tumor resections are some of the most critical and precision demanding procedures that might benefit from the proposed approach. However, this can be sometimes time consuming and/or not very effective when large environmental deformations occur during the surgical

[2]We note that the VF generation time is negligible with respect to recording phase, thus we can assume it is an instantaneous process.

procedure. In this case, vision systems might be adopted to increase the efficacy of the proposed method [3]. They can also be useful for the constraint enforcement definition: for instance, to estimate a complex surface normal direction to be left free. In any case, aside the methodology used for VF generation/update, the developed passivity-based control technique can be equally applied.

VI. Conclusions and Future Works

In this paper, we have introduced and experimentally validated a methodology to generate and adapt VF pose and geometry in robot-aided minimally invasive surgical tasks. The methodology relies on a VF generation strategy in which recorded interaction points are used to create the constraint geometry. Pose and geometry adaptation strategies have been developed to allow flexible use of VF assistance. Energy tanks passivity-based control has been proposed to guarantee a stable behavior of the system. The devised strategies have been validated through experiments on the dVRK and have demonstrated stable and smooth behaviors.

Our aim for the future is to combine the proposed adaptation strategies with task encoding and/or vision-based tracking methods for automatic VF switching/update. A human-subject evaluation involving novice and expert surgeons will be conducted to assess the effectiveness of our method. Ultimately, we will consider the generalization to other robotic surgical tasks, such as suturing [35]. We believe that the proposed methodology may leverage the development of next generation assistive surgical systems that enable more precise and safer interventions.

References

[1] N. Enayati, E. D. Momi, and G. Ferrigno, "Haptics in robot-assisted surgery: Challenges and benefits," *IEEE Rev. Biomed. Eng.*, vol. 9, pp. 49–65, 2016.

[2] S. A. Bowyer, B. L. Davies, and F. R. y Baena, "Active constraints/virtual fixtures: A survey," *IEEE Trans. Robot.*, vol. 30, no. 1, pp. 138–157, 2014.

[3] M. Selvaggio, G. Notomista, F. Chen, B. Gao, F. Trapani, and D. Caldwell, "Enhancing bilateral teleoperation using camera-based online virtual fixtures generation," in *IEEE/RSJ Int. Conf. on Intelligent Robots and Systems*, 2016, pp. 1483–1488.

[4] M. Selvaggio, F. Chen, B. Gao, G. Notomista, F. Trapani, and D. Caldwell, "Vision based virtual fixture generation for teleoperated robotic manipulation," in *Int. Conf. on Advanced Robotics and Mechatronics*, 2016, pp. 190–195.

[5] L. Wang, Z. Chen, P. Chalasani, R. M. Yasin, P. Kazanzides, R. H. Taylor, and N. Simaan, "Force-controlled exploration for updating virtual fixture geometry in model-mediated telemanipulation," *ASME Journal of Mechanisms Robotics*, vol. 9, pp. 021 010–11, 2017.

[6] F. Ferraguti, C. Secchi, and C. Fantuzzi, "A tank-based approach to impedance control with variable stiffness," in *IEEE Int. Conf. on Robotics and Automation*, 2013, pp. 4948–4953.

[7] C. T. Landi, F. Ferraguti, L. Sabattini, C. Secchi, and C. Fantuzzi, "Admittance control parameter adaptation for physical human-robot interaction," in *IEEE Int. Conf. on Robotics and Automation*, 2017, pp. 2911–2916.

[8] L. B. Rosenberg, "Virtual fixtures: Perceptual tools for telerobotic manipulation," in *IEEE Virtual Reality Annual International Symposium*, 1993, pp. 76–82.

[9] S. Park, R. D. Howe, and D. F. Torchiana, "Virtual fixtures for robotic cardiac surgery," in *Medical Image Computing and Computer-Assisted Intervention*. Springer Berlin Heidelberg, 2001, pp. 1419–1420.

[10] M. Li, A. Kapoor, and R. H. Taylor, *Telerobotic Control by Virtual Fixtures for Surgical Applications*. Springer Berlin Heidelberg, 2007, pp. 381–401.

[11] A. Bettini, S. Lang, A. M. Okamura, and G. D. Hager, "Vision assisted control for manipulation using virtual fixtures," in *IEEE/RSJ Int. Conf. on Intelligent Robots and Systems, 2001*, pp. 1171–1176.

[12] M. Li, M. Ishii, and R. H. Taylor, "Spatial motion constraints using virtual fixtures generated by anatomy," *IEEE Trans. Robot.*, vol. 23, no. 1, pp. 4–19, 2007.

[13] D. Zhang, Q. Zhu, J. Xiong, and L. Wang, "Dynamic virtual fixture on the euclidean group for admittance-type manipulator in deforming environments," *Biomed Eng Online*, vol. 13, no. 1, p. 51, 2014.

[14] D. Aarno, S. Ekvall, and D. Kragic, "Adaptive virtual fixtures for machine-assisted teleoperation tasks," in *IEEE Int. Conf. on Robotics and Automation*, 2005, pp. 1139–1144.

[15] M. Shahbazi, S. F. Atashzar, and R. V. Patel, "A dual-user teleoperated system with virtual fixtures for robotic surgical training," in *IEEE Int. Conf. on Robotics and Automation*, 2013, pp. 3639–3644.

[16] P. Marayong and A. M. Okamura, "Speed-accuracy characteristics of human-machine cooperative manipulation using virtual fixtures with variable admittance," *Human Factors*, vol. 46, no. 3, pp. 518–532, 2004.

[17] S. Ekvall, D. Aarno, and D. Kragic, "Online task recognition and real-time adaptive assistance for computer-aided machine control," *IEEE Trans. Robot.*, vol. 22, no. 5, pp. 1029–1033, 2006.

[18] N. Enayati, E. C. A. Costa, G. Ferrigno, and E. D. Momi, "A dynamic non-energy-storing guidance constraint with motion redirection for robot-assisted surgery," in *IEEE/RSJ Int. Conf. on Intelligent Robots and Systems*, 2016, pp. 4311–4316.

[19] S. A. Bowyer and F. R. y Baena, "Dynamic frictional constraints for robot assisted surgery," in *World Haptics Conference*, 2013, pp. 319–324.

[20] F. Ferraguti, N. Preda, M. Bonfè, and C. Secchi, "Bilateral teleoperation of a dual arms surgical robot with passive virtual fixtures generation," in *IEEE/RSJ Int. Conf. on Intelligent Robots and Systems*, 2015, pp. 4223–4228.

[21] A. Toedtheide, E. Shahriari, and S. Haddadin, "Tank based unified torque/impedance control for a pneumatically actuated antagonistic robot joint," in *IEEE Int. Conf. Robot. Autom.*, 2017, pp. 1255–1262.

[22] P. Kazanzides, Z. Chen, A. Deguet, G. S. Fischer, R. H. Taylor, and S. P. DiMaio, "An open-source research kit for the da vinci surgical system," in *IEEE Int. Conf. on Robotics and Automation*, 2014, pp. 6434–6439.

[23] B. Siciliano, L. Sciavicco, L. Villani, and G. Oriolo, *Robotics: Modelling, Planning and Control*. Springer, 2010.

[24] A. D. Luca and R. Mattone, "Actuator failure detection and isolation using generalized momenta," in *IEEE Int. Conf. on Robotics and Automation*, 2003, pp. 634–639.

[25] A. D. Luca and R. Mattone, "Sensorless robot collision detection and hybrid force/motion control," in *IEEE Int. Conf. on Robotics and Automation*, 2005, pp. 999–1004.

[26] C. Secchi, S. Stramigioli, and C. Fantuzzi, "Position drift compensation in port-hamiltonian based telemanipulation," in *IEEE/RSJ Int. Conf. on Intelligent Robots and Systems*, 2006, pp. 4211–4216.

[27] D. Lee and K. Huang, "Passive-set-position-modulation framework for interactive robotic systems," *IEEE Trans. Robot.*, vol. 26, no. 2, pp. 354–369, April 2010.

[28] G. A. Fontanelli, F. Ficuciello, L. Villani, and B. Siciliano, "Modelling and identification of the da vinci research kit robotic arms," in *IEEE/RSJ Int. Conf. on Intelligent Robots and Systems*, 2017, pp. 1464–1469.

[29] P. Kazanzides, Z. Chen, A. Deguet, G. S. Fischer, R. H. Taylor, and S. P. DiMaio, "An open-source research kit for the da vinci surgical system," in *IEEE Int. Conf. on Robotics and Automation*, 2014, pp. 6434–6439.

[30] G. A. Fontanelli, L. R. Buonocore, F. Ficuciello, L. Villani, and B. Siciliano, "A novel force sensing integrated into the trocar for minimally invasive robotic surgery," in *2017 IEEE/RSJ Int. Conf. on Intelligent Robots and Systems*, 2017, pp. 131–136.

[31] S. Bochkanov. Alglib. [Online]. Available: www.alglib.net

[32] G. A. Fontanelli, M. Selvaggio, M. Ferro, F. Ficuciello, M. Vendittelli, and B. Siciliano, "A v-rep simulator for the da vinci research kit robotic platform," in *7th IEEE RAS/EMBS Int. Conf. on Biomedical Robotics and Biomechatronics*, 2018.

[33] K. Kronander and A. Billard, "Stability considerations for variable impedance control," *IEEE Trans. Robot.*, vol. 32, no. 5, pp. 1298–1305, 2016.

[34] B. Hannaford and J.-H. Ryu, "Time-domain passivity control of haptic interfaces," *IEEE Trans. Robot. Autom.*, vol. 18, no. 1, pp. 1–10, 2002.

[35] G. A. Fontanelli, M. Selvaggio, L. R. Buonocore, F. Ficuciello, L. Villani, and B. Siciliano, "A new laparoscopic tool with in-hand rolling capabilities for needle reorientation," *IEEE Robotics and Automation Letters*, vol. 3, no. 3, pp. 2354–2361, 2018.